January 2014

Sediment Profile Imaging Report

Demonstration of *in-situ* Treatment of Contaminated Sediments with Reactive Amendments: Post-Cap Survey #2




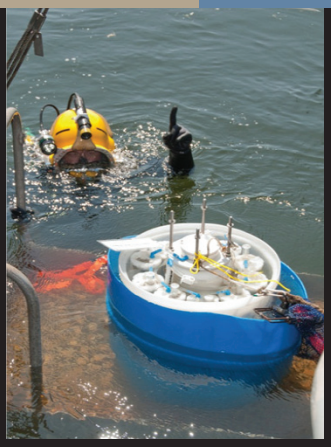


Prepared for

Hart Crowser, Inc.
1700 Westlake Avenue North
Suite 200
Seattle, WA 98109-3856

Hart Crowser Job Number 1789701,
Work Order #1

Prepared by

Germano & Associates, Inc.
12100 SE 46th Place
Bellevue, WA 98006

Sediment Profile Imaging Report

DEMONSTRATION OF *IN-SITU* TREATMENT OF CONTAMINATED SEDIMENTS WITH REACTIVE AMENDMENTS: POST CAP SURVEY #2

Prepared for

Hart Crowser, Inc.
1700 Westlake Avenue North, Suite 200
Seattle, WA 98109-3856

Hart Crowser Job Number 1789701, Work Order #1

Prepared by

Germano & Associates, Inc.
12100 SE 46th Place
Bellevue, WA 98006

January, 2014

TABLE OF CONTENTS

LIST OF FIGURES ..... **iii**

1.0 INTRODUCTION **1**

2.0 MATERIALS AND METHODS **2**

2.1 MEASURING, INTERPRETING, AND MAPPING SPI PARAMETERS 4
2.1.1 Prism Penetration Depth *4*
2.1.2 Thickness of Depositional Layers *5*
2.1.3 Apparent Redox Potential Discontinuity Depth *5*
2.1.4 Infaunal Successional Stage *7*
2.1.5 Biological Mixing Depth *8*

3.0 RESULTS **10**

3.1 PRISM PENETRATION DEPTH 11
3.2 THICKNESS OF REACTIVE AMENDMENT LAYER 11
3.3 APPARENT REDOX POTENTIAL DISCONTINUITY DEPTH 11
3.4 INFAUNAL SUCCESSIONAL STAGE 11
3.5 MAXIMUM BIOLOGICAL MIXING DEPTH 12

4.0 DISCUSSION **13**

5.0 REFERENCES CITED **14**

FIGURES

APPENDIX A: Sediment Profile Image Analysis Results

LIST OF FIGURES

Figure 1 Spatial distribution and average depositional thickness (cm) of the AquaGate +PAC^{TM} material placed at locations in and around Pier 7 at the PSNS & IMF Bremerton site in October, 2012.

Figure 2 Location of SPI stations under and around Pier 7 at PSNS & IMF, Bremerton site in August 2013.

Figure 3 Deployment and operation of the SPI camera system.

Figure 4 The hand-held SPI system used by divers for all stations that were located underneath Pier 7 at PSNS & IMF, Bremerton site.

Figure 5 The stages of infaunal succession as a response of soft-bottom benthic communities to physical disturbance (top panel) or organic enrichment (bottom panel).

Figure 6 These profile images taken with the hand-held camera under the pier from Station 01-1 (left) and Station 06-1 (right) show the unusually high percentage of shell fragments mixed in with the silt-clay sediments

Figure 7 These profile images from Stations 1-3 (left) and 3-3 (right) show a shell and cobble armoring layer over the ambient fine sediments.

Figure 8 These profile images from the same stations taken in 2012 and 2013 show the radical change in sediment type because of the appearance of the surface armoring of cobble and shell.

Figure 9 Spatial distribution of mean camera prism penetration depth (cm) at Pier 7 at the PSNS & IMF Bremerton site in August, 2013.

Figure 10 This profile image from Station 5-3 (use rep C) shows a distinct layer of the white pebbles that were coated with the reactive amendment and used as a carrier to get the material to the bottom sediments; particles of activated carbon are still visible in the subsurface profile.

Figure 11 Spatial distribution and mean depositional thickness (cm) of the AquaGate +PAC^{TM} material placed at locations in and around Pier 7 at the PSNS & IMF Bremerton site.

Figure 12 Spatial distribution of mean apparent RPD depth (cm) at Pier 7 in August, 2013.

Figure 13 Spatial distribution of infaunal successional stages at Pier 7 at the PSNS & IMF Bremerton site in August, 2013.

Figure 14 Spatial distribution of maximum biological mixing depth at Pier 7 at the PSNS & IMF Bremerton site in August, 2013.

Figure 15 This profile image from Station 4-4 shows active particle transport of the activated carbon particles as well as the development of a surface oxidized layer.

Figure 16 These profile images from Stations 3-4 (top) and 4-2 (bottom) show an obvious presence of the reactive amendment in 2012 that seems to no longer be present in 2013.

Figure 17 These profile images from 2012 and 2013 at Station 6-4 show the small-scale heterogeneity in the spatial distribution of the reactive amendment added in Oct 2012.

1.0
INTRODUCTION

As part of a multidisciplinary effort to investigate the feasibility of treating contaminated sediments in active Department of Defense (DoD) harbors, Germano & Associates, Inc. (G&A) performed a Sediment Profile Imaging (SPI) survey around Pier 7 at the Puget Sound Naval Shipyard & Intermediate Maintenance Facility (PSNS & IMF) Bremerton site. The purpose of this SPI survey was to document conditions at a total of 50 stations following placement of a reactive amendment cap placed on the sediment surface.

2.0
MATERIALS AND METHODS

Between October 14-16, 2012, 141 tons of AquaGate +PAC^{TM} were placed in the target area for remediation under and around Pier 7 at PSNS & IMF Bremerton site (Johnston et al. 2013). An initial post-placement SPI survey was performed on October 30-31, 2012, 2 weeks after the capping operation was finished. Scientists from G&A collected a series of sediment profile images at a total of 42 stations (Germano and Associates, 2013) and mapped the presence and thickness of the cap layer (Figure 1). Approximately one year later, on August 13-14, 2013, scientists from G&A collected sediment profile images from the same 42 stations as well as an additional 8 stations (Figure 2) to monitor the recolonization of the cap as well as the active reworking of the reactive amendment into the sediment by resident infauna. On both surveys, two different versions of an Ocean Imaging Systems Model 3731 sediment profile camera were used; a standard SPI system using a surrounding frame that was deployed from a vessel (Figure 3), and a hand-held aluminum SPI system (Figure 4) deployed by PSNS & IMF divers for stations that were located under the pier and inaccessible for sampling with a boat.

SPI was developed almost four decades ago as a rapid reconnaissance tool for characterizing physical, chemical, and biological seafloor processes and has been used in numerous seafloor surveys throughout North America, Asia, Europe, and Africa (Rhoads and Germano 1982, 1986, 1990; Revelas et al. 1987; Diaz and Schaffner, 1988; Valente et al. 1992; Germano et al. 2011). The sediment profile camera works like an inverted periscope. A Nikon D7000 16.2-megapixel SLR camera with two 8-gigabyte secure digital (SD) cards is mounted horizontally inside a watertight housing on top of a wedge-shaped prism. The prism has a Plexiglas® faceplate at the front with a mirror placed at a 45° angle at the back. The camera lens looks down at the mirror, which is reflecting the image from the faceplate. The prism has an internal strobe mounted inside at the back of the wedge to provide illumination for the image; this chamber is filled with distilled water, so the camera always has an optically clear path. This wedge assembly is mounted on a moveable carriage within a stainless steel frame. The frame is lowered to the seafloor on a winch wire, and the tension on the wire keeps the prism in its “up” position. When the frame comes to rest on the seafloor, the winch wire goes slack (see Figure 3) and the camera prism descends into the sediment at a slow, controlled rate by the dampening action of a hydraulic piston so as not to disturb the sediment-water interface. On the way down, it trips a trigger that activates a time-delay circuit of variable length (operator-selected) to allow the camera to penetrate the seafloor before any image is taken. The knife-sharp edge of the prism transects the sediment, and the prism penetrates the bottom. The strobe is discharged after an appropriate time delay to obtain a cross-sectional image of the upper 20 cm of the sediment column. The resulting images give the viewer the same perspective as looking through the side of an aquarium half-filled with sediment. After the first image is obtained at the first location, the camera is then

raised up about 2 to 3 meters off the bottom to allow the strobe to recharge; a wiper blade mounted on the frame removes any mud adhering to the faceplate. The strobe recharges within 5 seconds, and the camera is ready to be lowered again for a replicate image. Surveys can be accomplished rapidly by "pogo-sticking" the camera across an area of seafloor while recording positional fixes on the surface vessel.

The hand-held SPI system (Figure 4) works on the same design, except that there is no time delay once the watertight switch is activated by the diver after the prism is inserted into the sediment. There is no wiper blade on the hand-held system, so the diver needs to clean the faceplate of the camera prism manually with a scrub brush after each image is taken.

Two types of adjustments to the SPI system are typically made in the field: physical adjustments to the chassis stop collars on the frame-deployed system or adding/subtracting lead weights to the chassis to control penetration in harder or softer sediments, and electronic software adjustments to the Nikon D7000 to control camera settings. Camera settings (f-stop, shutter speed, ISO equivalents, digital file format, color balance, etc.) are selectable through a water-tight USB port on the camera housing and Nikon Control Pro® software. At the beginning of the survey, the time on both of the sediment profile cameras' internal data loggers was synchronized with the clock on the sampling vessel to local time. Details of the camera settings for each digital image are available in the associated parameters file embedded in the electronic image file; for this survey, the ISO-equivalent was set at 640. The additional camera settings used were as follows: shutter speed was 1/250, f8, white balance set to flash, color mode to Adobe RGB, sharpening to none, noise reduction off, and storage in compressed raw Nikon Electronic Format (NEF) files (approximately 20 MB each). Electronic files were converted to high-resolution jpeg (14-bit) format files (49278 x 3264 pixels) using Nikon Capture NX2® software (Version 2.3.5.).

Three replicate images were taken at each station at the vessel-deployed frame stations, while 2 replicate images were taken by the divers at each of the under-pier stations; each SPI replicate is identified by the time recorded on the digital image file in the camera and in the field log on the vessel. The SD card was immediately surrendered at the completion of the survey to PSNS & IMF for review and approval for public distribution. The unique time stamp on the digital image was then cross-checked with the time stamp recorded in the written sample logs. After the images were cleared for public release, they were re-named with the appropriate station name based on the time stamp on each image.

Test exposures of the Kodak® Color Separation Guide (Publication No. Q-13) were made on deck at the beginning of the survey to verify that all internal electronic systems were working to design specifications and to provide a color standard against which final images could be checked for proper color balance. A spare camera and charged battery were carried in the field at all times to insure uninterrupted sample acquisition. After

deployment of the camera at each station, the frame counter was checked to make sure that the requisite number of replicates had been taken. In addition, a prism penetration depth indicator on the camera frame was checked to verify that the optical prism had actually penetrated the bottom to a sufficient depth. If images were missed (frame counter indicator or verification from digital download) or the penetration depth was insufficient (penetration indicator), chassis stops were adjusted and/or weights were added or removed, and additional replicate images were taken. Changes in prism weight amounts, the presence or absence of mud doors, and chassis stop positions were recorded for each replicate image.

Following completion of the field operations, the raw NEF image files were converted to high-resolution Joint Photographic Experts Group (jpeg) format files using the minimal amount of image file compression. Once converted to jpeg format, the intensity histogram (RGB channel) for each image was adjusted in Adobe Photoshop® to maximize contrast without distortion. The jpeg images were then imported to Sigmascan Pro® (Aspire Software International) for image calibration and analysis. Calibration information was determined by measuring 1-cm gradations from the Kodak® Color Separation Guide. This calibration information was applied to all SPI images analyzed. Linear and area measurements were recorded as number of pixels and converted to scientific units using the calibration information.

Measured parameters were recorded on a Microsoft® Excel© spreadsheet. G&A's senior scientist (Dr. J. Germano) subsequently checked all these data as an independent quality assurance/quality control review of the measurements before final interpretation was performed.

2.1 MEASURING, INTERPRETING, AND MAPPING SPI PARAMETERS

2.1.1 Prism Penetration Depth

The SPI prism penetration depth was measured from the bottom of the image to the sediment-water interface. The area of the entire cross-sectional sedimentary portion of the image was digitized, and this number was divided by the calibrated linear width of the image to determine the average penetration depth.

Prism penetration is a noteworthy parameter; if the number of weights used in the camera is held constant throughout a survey, the camera functions as a static-load penetrometer. Comparative penetration values from sites of similar grain size give an indication of the relative water content of the sediment. Highly bioturbated sediments and rapidly accumulating sediments tend to have the highest water contents and greatest prism penetration depths.

The depth of penetration also reflects the bearing capacity and shear strength of the sediments. Overconsolidated or relic sediments and shell-bearing sands resist camera penetration. Highly bioturbated, sulfitic, or methanogenic muds are the least consolidated, and deep penetration is typical. Seasonal changes in camera prism penetration have been observed at the same station in other studies and are related to the control of sediment geotechnical properties by bioturbation (Rhoads and Boyer 1982). The effect of water temperature on bioturbation rates appears to be important in controlling both biogenic surface relief and prism penetration depth (Rhoads and Germano 1982).

2.1.2 Thickness of Depositional Layers

Because of the camera's unique design, SPI can be used to detect the thickness of dredged material and depositional layers (like the reactive amendment). SPI is effective in measuring layers ranging in thickness from 1 mm to 20 cm (the height of the SPI optical window). During image analysis, the thickness of the newly deposited sedimentary layers can be determined by measuring the distance between the pre- and post-disposal sediment-water interface. Recently deposited material is usually evident because of its unique optical reflectance and/or color relative to the underlying material representing the pre-disposal surface. Also, in most cases, the point of contact between the two layers is clearly visible as a textural change in sediment composition, facilitating measurement of the thickness of the newly deposited layer.

2.1.3 Apparent Redox Potential Discontinuity Depth

Aerobic near-surface marine sediments typically have higher reflectance relative to underlying hypoxic or anoxic sediments. Surface sands washed free of mud also have higher optical reflectance than underlying muddy sands. These differences in optical reflectance are readily apparent in SPI images; the oxidized surface sediment contains particles coated with ferric hydroxide (an olive or tan color when associated with particles), while reduced and muddy sediments below this oxygenated layer are darker, generally gray to black (Fenchel 1969; Lyle 1983). The boundary between the colored ferric hydroxide surface sediment and underlying gray to black sediment is called the apparent redox potential discontinuity (aRPD).

The depth of the aRPD in the sediment column is an important time-integrator of dissolved oxygen conditions within sediment porewaters. In the absence of bioturbating organisms, this high reflectance layer (in muds) will typically reach a thickness of 2 mm below the sediment-water interface (Rhoads 1974). This depth is related to the supply rate of molecular oxygen by diffusion into the bottom and the consumption of that oxygen by the sediment and associated microflora. In sediments that have very high sediment oxygen demand (SOD), the sediment may lack a high reflectance layer even when the overlying water column is aerobic.

In the presence of bioturbating macrofauna, the thickness of the high reflectance layer may be several centimeters. The relationship between the thickness of this high reflectance layer and the presence or absence of free molecular oxygen in the associated porewaters must be considered with caution. The actual RPD is the boundary or horizon that separates the positive reduction potential (Eh) region of the sediment column from the underlying negative Eh region. The exact location of this Eh = 0 boundary can be determined accurately only with microelectrodes; hence, the relationship between the change in optical reflectance, as imaged with the SPI camera, and the actual RPD can be determined only by making the appropriate *in situ* Eh measurements. For this reason, the optical reflectance boundary, as imaged, was described in this study as the "apparent" RPD and it was mapped as a mean value. In general, the depth of the actual Eh = 0 horizon will be either equal to or slightly shallower than the depth of the optical reflectance boundary (Rosenberg et al., 2001). This is because bioturbating organisms can mix ferric hydroxide-coated particles downward into the bottom below the Eh = 0 horizon. As a result, the mean aRPD depth can be used as an estimate of the depth of porewater exchange, usually through porewater irrigation (bioturbation). Biogenic particle mixing depths can be estimated by measuring the maximum and minimum depths of imaged feeding voids in the sediment column. This parameter represents the particle mixing depths of head-down feeders, mainly polychaetes.

The rate of depression of the aRPD within the sediment is relatively slow in organic-rich muds, on the order of 200 to 300 micrometers per day; therefore this parameter has a long time constant (Germano and Rhoads 1984). The rebound in the aRPD is also slow (Germano 1983). Measurable changes in the aRPD depth using the SPI optical technique can be detected over periods of 1 or 2 months. This parameter is used effectively to document changes (or gradients) that develop over a seasonal or yearly cycle related to water temperature effects on bioturbation rates, seasonal hypoxia, SOD, and infaunal recruitment. Time-series RPD measurements following a disturbance can be a critical diagnostic element in monitoring the degree of recolonization in an area by the ambient benthos (Rhoads and Germano 1986).

The mean aRPD depth also can be affected by local erosion. The peaks of disposal mounds commonly are scoured by divergent flow over the mound. This scouring can wash away fines and shell or gravel lag deposits, and can result in very thin surface oxidized layer. During storm periods, erosion may completely remove any evidence of the aRPD (Fredette et al. 1988).

Another important characteristic of the aRPD is the contrast in reflectance at this boundary. This contrast is related to the interactions among the degree of organic loading, the bioturbation activity in the sediment, and the concentrations of bottom-water dissolved oxygen in an area. High inputs of labile organic material increase SOD and, subsequently, sulfate reduction rates and the associated abundance of sulfide end products. This results in more highly reduced, lower-reflectance sediments at depth and higher aRPD contrasts. In a region of generally low aRPD contrasts, images with high

aRPD contrasts indicate localized sites of relatively large inputs of organic-rich material such as phytoplankton, other naturally-occurring organic detritus, dredged material, or sewage sludge.

Because the determination of the aRPD requires discrimination of optical contrast between oxidized and reduced particles, it is difficult, if not impossible, to determine the depth of the aRPD in well-sorted sands of any size that have little to no silt or organic matter in them (Painter et al, 2007). When using SPI technology on sand bottoms, little information other than grain-size, prism penetration depth, and boundary roughness values can be measured; while oxygen has no doubt penetrated the sand beneath the sediment-water interface just due to physical forcing factors acting on surface roughness elements (Ziebis et al., 1996; Huettel et al., 1998), estimates of the mean aRPD depths in these types of sediments are indeterminate with conventional white light photography.

2.1.4 Infaunal Successional Stage

The mapping of infaunal successional stages is readily accomplished with SPI technology. These stages are recognized in SPI images by the presence of dense assemblages of near-surface polychaetes and/or the presence of subsurface feeding voids; both may be present in the same image. Mapping of successional stages is based on the theory that organism-sediment interactions in fine-grained sediments follow a predictable sequence after a major seafloor perturbation. This theory states that primary succession results in "the predictable appearance of macrobenthic invertebrates belonging to specific functional types following a benthic disturbance. These invertebrates interact with sediment in specific ways. Because functional types are the biological units of interest..., our definition does not demand a sequential appearance of particular invertebrate species or genera" (Rhoads and Boyer 1982). This theory is presented in Pearson and Rosenberg (1978) and further developed in Rhoads and Germano (1982) and Rhoads and Boyer (1982).

This continuum of change in animal communities after a disturbance (primary succession) has been divided subjectively into four stages: Stage 0, indicative of a sediment column that is largely devoid of macrofauna, occurs immediately following a physical disturbance or in close proximity to an organic enrichment source; Stage 1 is the initial community of tiny, densely populated polychaete assemblages; Stage 2 is the start of the transition to head-down deposit feeders; and Stage 3 is the mature, equilibrium community of deep-dwelling, head-down deposit feeders (Figure 5).

After an area of bottom is disturbed by natural or anthropogenic events, the first invertebrate assemblage (Stage 1) appears within days after the disturbance. Stage 1 consists of assemblages of tiny tube-dwelling marine polychaetes that reach population densities of 10^4 to 10^6 individuals per m^2. These animals feed at or near the sediment-water interface and physically stabilize or bind the sediment surface by producing a mucous "glue" that they use to build their tubes. Sometimes deposited dredged material

layers contain Stage 1 tubes still attached to mud clasts from their location of origin; these transported individuals are considered as part of the *in situ* fauna in our assignment of successional stages.

If there are no repeated disturbances to the newly colonized area, then these initial tube-dwelling suspension or surface-deposit feeding taxa are followed by burrowing, head-down deposit-feeders that rework the sediment deeper and deeper over time and mix oxygen from the overlying water into the sediment. The animals in these later-appearing communities (Stage 2 or 3) are larger, have lower overall population densities (10 to 100 individuals per m^2), and can rework the sediments to depths of 3 to 20 cm or more. These animals "loosen" the sedimentary fabric, increase the water content in the sediment, thereby lowering the sediment shear strength, and actively recycle nutrients because of the high exchange rate with the overlying waters resulting from their burrowing and feeding activities.

In dynamic estuarine and coastal environments, it is simplistic to assume that benthic communities always progress completely and sequentially through all four stages in accordance with the idealized conceptual model depicted in Figure 3. Various combinations of these basic successional stages are possible. For example, secondary succession can occur (Horn, 1974) in response to additional labile carbon input to surface sediments, with surface-dwelling Stage 1 or 2 organisms co-existing at the same time and place with Stage 3, resulting in the assignment of a "Stage 1 on 3" or "Stage 2 on 3" designation.

While the successional dynamics of invertebrate communities in fine-grained sediments have been well-documented, the successional dynamics of invertebrate communities in sand and coarser sediments are not well-known. Subsequently, the insights gained from sediment profile imaging technology regarding biological community structure and dynamics in sandy and coarse-grained bottoms are fairly limited.

2.1.5 Biological Mixing Depth

During the past two decades, there has been a considerable emphasis on studying the effects of bioturbation on sediment geotechnical properties as well as sediment diagenesis (Ekman et al., 1981; Nowell et al., 1981; Rhoads and Boyer, 1982; Grant et al., 1982; Boudreau, 1986; 1994; 1998). However, an increasing focus of research is centering on the rates of contaminant flux in sediments (Reible and Thibodeaux, 1999; François et al., 2002; Gilbert et al., 2003), and the two parameters that affect the time rate of contaminant flux the greatest are erosion and bioturbation (Reible and Thibodeaux, 1999). The depth to which sediments are bioturbated, or the biological mixing depth, can be an important parameter for studying either nutrient or contaminant flux in sediments. While the apparent RPD is one potential measure of biological mixing depth, it is quite common in profile images to see evidence of biological activity (burrows, voids, or actual animals)

well below the mean apparent RPD. Both the minimum and maximum linear distance from the sediment surface to both the shallowest and deepest feature of biological activity can be measured along with a notation of the type of biogenic structure measured. For this report, the maximum depth to which any biological activity was noted was measured and mapped.

.

3.0
RESULTS

While replicate images were taken at each station, the amount of disturbance caused by the diver-deployed system did not allow for reliable measurements of precision between the two replicate images, so only one replicate (the least disturbed) from each station sampled by divers was analyzed. The amount of debris in and around the piers coupled with the high density of shell fragments also created high variation in the penetration depth at the frame deployed stations, with cross-sectional sedimentary structures masked or destroyed by debris (natural or anthropogenic) being dragged down by the prism cutting blade. While a copy of all images collected was provided to the client, given the variation in image feature preservation (regardless of whether they were taken with the frame-deployed or diver-deployed system), and because this variation in cross-sectional structural appearance was not really indicative of natural variance in the measured parameters, the best image (least disturbed) from each station was analyzed. A complete set of all the summary data measured from each image is presented in Appendix A.

The results for some SPI parameters are sometimes indicated in the data appendix or on the maps as being "Indeterminate" (Ind). This is a result of the sediments being either: 1) too compact for the profile camera to penetrate adequately, preventing observation of surface or subsurface sediment features, 2) too soft to bear the weight of the camera, resulting in over-penetration to the point where the sediment/water interface was above the window (imaging area) on the camera prism (the sediment/water interface must be visible to measure most of the key SPI parameters like aRPD depth, penetration depth, and infaunal successional stage), or 3) the biogenic and sedimentary stratigraphic structure was compromised or destroyed by sampling artifacts caused by the divers inserting the prism into the sediment (either vibrating or wiggling the camera to achieve greater penetration, which allowed suspended sediment to collect in between the cross-sectional profile and the faceplate of the prism)

SPI has been shown to be a powerful reconnaissance tool that can efficiently map gradients in sediment type, biological communities, or disturbances from physical forces or organic enrichment. The results and conclusions in this report are about dynamic processes that have been deduced from imaged structures; as such, they should be considered hypotheses available for further testing/confirmation. By employing Occam's Razor, we feel reasonably assured that the most parsimonious explanation is usually the one borne out by subsequent data confirmation

3.1 PRISM PENETRATION DEPTH

Sediments throughout the site ranged from sandy silt to muds with minor fractions of very fine to fine sand with high percentages of shell hash (stations under Pier 7; see Figure 6) to pebble and cobble armoring over silty sands (Figure 7). As noted from the results of the survey done last year in October right after the capping operation, the addition of the AquaGate amendment also provided some surface armoring at select stations which impeded camera prism penetration. There was a noticeable decrease in prism penetration depth at the stations along the western edge of the pier compared with the results from last year; the cobble/shell armoring (Figure 7) appears to have been deposited at some point in the last 12 months and extends in a linear fashion from Station 1-3 south to Station 4-3 (Figure 8). The mean prism penetration depth in the study area ranged from 1.6 to 20.4 cm, with an overall site average of 12.1 cm; the spatial distribution of mean penetration depth at all stations sampled is shown in Figure 9.

3.2 THICKNESS OF REACTIVE AMENDMENT LAYER

Measureable deposits of AquaGate+PAC^{TM} could be seen at 16 stations, while 5 stations showed only traces of the AquaGate particles in the upper oxidized layer of sediment (Figure 10). At those stations where the cap material could be detected, the mean thickness ranged from trace layers to 18.3 cm, with an average thickness of 8.0 cm at those 16 stations where a distinct layer could be measured. The footprint of the cap is shown in Figure 11.

3.3 APPARENT REDOX POTENTIAL DISCONTINUITY DEPTH

The distribution of mean apparent RPD depths is shown in Figure 12; mean aRPD depths could not be measured at 7 of the stations sampled by divers because of sampling artifacts that caused distortions to the sediment profile and eliminated the possibility of any accurate measurements; cobble/shell at two of the stations (Stations 1-3 and 3-3) prevented sufficient prism penetration to get an aRPD measurement. While eight of the stations still had no detectable aRPD present, the remaining stations had values ranging from 0.1 to 4.5 cm (Figure 12; Appendix A), with an overall site average of 1.4 cm.

3.4 INFAUNAL SUCCESSIONAL STAGE

The mapped distribution of infaunal successional stages is shown in Figure 13; while there was a noticeable improvement in biological community status under the pier compared to the post capping survey last year, there was a retrograde in successional status at some of the stations outboard of the pier (Stations 1-5, 1-6, 2-4, 2-6, 3-4, and 3-

6). However, presence of Stage 3 taxa (larger infaunal deposit feeders) was evident at 18 of the 50 stations.

3.5 MAXIMUM BIOLOGICAL MIXING DEPTH

The spatial distribution of the maximum depth to which any biological activity was seen in the study area is shown in Figure 14. Some of the deepest infaunal burrowing was found at those stations under the pier where the reactive amendment had been placed; maximum depth of biogenic activity ranged from 0.9 to 18.7 cm, with an overall site average of 10.2 cm.

4.0
DISCUSSION

There were some substantial change to seafloor conditions compared with those from last October (Germano & Associates 2013). While the appearance of the cobble armoring layer (Figures 7-8) just to the western outboard edge of Pier 7 was somewhat unexpected, it was particularly gratifying to obtain visual evidence of the reactive amendment being re-worked into the bottom sediments by bioturbation as originally planned (Figure 15). Another unexpected result was the apparent small-scale heterogeneity in some of the mapped patterns of reactive amendment from 2012 (Figure 1) to 2013 (Figure 11). There were some locations where the layer that was obvious in 2012 was no longer visible in 2013 (Figure 16), and conversely where there was no detectable layer in 2012 appeared to be present in 2013 (Figure 17).

The results from this survey showed that activated cap amendment is definitely being reworked into the sediments by the resident infauna; over time, the re-appearance of Stage 3 taxa as well as thicker oxidized surface (aRPD) layers should be more widespread (depending on the frequency of physical disturbance to the bottom from propwash and ship traffic activity)

There was also a noticeable improvement in the image quality from locations sampled with the hand-held camera; the PSNS & IMF Bremerton site divers have definitely improved their technique with the experience gained from the first two efforts. We would like to acknowledge both their attention to safety and skill in sample collection; it is truly a pleasure to collaborate with them and the rest of the PSNS & IMF Bremerton site personnel on this project.

5.0
REFERENCES CITED

Boudreau, B.P. 1986. Mathematics of tracer mixing in sediment. I-Spatially-dependent, diffusive mixing. II: Non-local mixing and biological conveyor-belt phenomena. Am. Jour. Sci. 286: 161-238.

Boudreau, B.P. 1994. Is burial velocity a master parameter for bioturbation? Geochimica et Cosmochemica Acta 58: 1243-1249.

Boudreau, B. P. 1998. Mean mixed depth of sediments: The wherefore and the why. Limnol. Oceanogr. 43: 524-526.

Diaz, R. J. and L. C. Schaffner. 1988. Comparison of sediment landscapes in the Chesapeake Bay as seen by surface and profile imaging, p. 222-240 In M. P. Lynch and E. C. Krome (eds.), Understanding the Estuary: Advances in Chesapeake Bay Research, Chesapeake Bay Research Consortium Publication 129, Chesapeake Bay Program 24/88.

Ekman, J.E., Nowell, A.R.M., and P.A. Jumars. 1981. Sediment destabilization by animal tubes. J. Mar. Res. 39: 361-374.

Fenchel, T. 1969. The ecology of marine macrobenthos IV. Structure and function of the benthic ecosystem, its chemical and physical factors and the microfauna communities with special reference to the ciliated protozoa. Ophelia 6: 1-182.

François, F., Gerino, M., Stora, G., Durbec, J.P., and J.C. Poggiale. 2002. Functional approach to sediment reworking by gallery-forming macrobenthic organisms: modeling and application with the polychaete *Nereis diversicolor*. Marine Ecology Progress Series 229: 127–136.

Fredette, T.J., W.F. Bohlen, D.C. Rhoads, and R.W. Morton. 1988. Erosion and resuspension effects of Hurricane Gloria at Long Island Sound dredged material disposal sites. In: Proceedings of the Water Quality ‘88 seminar, February Meeting, Charleston, South Carolina. U.S. Army Corps of Engineers, Hydraulic Engineering Center, Davis, CA.

Germano, J.D. 1983. Infaunal succession in Long Island Sound: Animal-sediment interactions and the effects of predation. Ph.D. dissertation. Yale University, New Haven, CT. 206 pp.

Germano & Associates 2013. Demonstration of *in-situ* treatment of contaminated sediments with reactive amendments: Post Cap Survey #1. Final report submitted to Hart Crowser, Inc. Seattle, WA.

Germano, J.D. and D.C. Rhoads. 1984. REMOTS sediment profiling at the Field Verification Program (FVP) Disposal Site. In: Dredging '84 Proceedings, ASCE, Nov. 14-16, Clearwater, FL. pp. 536-544.

Germano, J.D., D.C. Rhoads, R.M. Valente, D.A. Carey, and M. Solan. 2011. The use of Sediment Profile Imaging (SPI) for environmental impact assessments and monitoring studies – lessons learned from the past four decades. Oceanography and Marine Biology: An Annual Review 49: 247-310.

Gilbert, F. S. Hulth, N. Strömberg, K. Ringdahl, and J.-C. Poggiale. 2003. 2-D optical quantification of particle reworking activities in marine surface sediments. Jour. Exp. Mar. Biol. Ecol. 285-286: 251-264.

Grant, W.D., Jr., Boyer, L.F., and Sanford, L.P. 1982. The effects of bioturbation on the initiation of motion of intertidal sands: Jour. Mar. Res., Vol. 40, pp. 659-677.

Horn, H.S. 1974. The ecology of secondary succession. Ann. Rev. Ecol. Syst. 5: 25-37.

Huettel, M., Ziebis, W., Forster., S., and G.W. Luther III. 1998. Advective transport affecting metal and nutrient distributions and interfacial fluxes in permeable sediments. Geochimica et Cosmochemica Acta 62: 613-631.

Johnston, R.K., V. Kirtay, D.B. Chadwick, G.H. Rosen, J.M. Guerrero, J. Collins, C. Ortega, R. Webb, R,. May, J. Germano, D. Browning, E. Beaver, M. Wicklein, J. Pittz, D.E. Leisle, L. Doyle, and L. Hsu. 2013. Installing an activated-carbon sediment amendment at the Puget Sound Naval Shipyard and Intermediate Maintenance Facility, Bremerton, WA. Paper B-024, Proceedings of the Seventh International Conference on Remediation of Contaminated Sediments (Dallas, TX; February 4-7, 2013). ISBN 978-0-9818730-6-7. ©2013 Battelle Memorial Institute, Columbus, OH. www.battelle.org/sedimentscon

Lyle, M. 1983. The brown-green colour transition in marine sediments: A marker of the Fe (III) – Fe(II) redox boundary. Limnol. Oceanogr. 28: 1026-1033.

Nowell, A.R.M., P.A. Jumars, and J.E. Ekman. 1981. Effects of biological activity on the entrainment of marine sediments. Mar. Geol. 42: 133-153.

Painter, T.H., M. E. Schaepman, W. Schweizer, and J. Brazile. 2007. Spectroscopic discrimination of shit from shinola. Annals of Improbable Research 13: 22-23.

Pearson, T.H. and R. Rosenberg. 1978. Macrobenthic succession in relation to organic enrichment and pollution of the marine environment. Oceanogr. Mar. Biol. Ann. Rev. 16:229-311.

Reible, D and Thibodeaux, L. 1999. Using Natural Processes to Define Exposure

From Sediments., in Sediment Management Work Group; Contaminated Sediment Management Technical Papers, Sediment Management Work Group, http://www.smwg.org/index.htm.

Revelas, E.C., J.D. Germano, and D.C. Rhoads. 1987. REMOTS reconnaissance of benthic environments. pp. 2069-2083. In: Coastal Zone '87 Proceedings, ASCE, WW Division, May 26-29, Seattle, WA.

Rhoads, D.C. 1974. Organism-sediment relations on the muddy seafloor. Oceanogr. Mar. Biol. Ann. Rev. 12: 263-300.

Rhoads, D.C. and L.F. Boyer. 1982. The effects of marine benthos on physical properties of sediments. pp. 3-52. In: Animal-Sediment Relations. McCall, P.L. and M.J.S. Tevesz (eds). Plenum Press, New York, NY.

Rhoads, D.C. and J.D. Germano. 1982. Characterization of benthic processes using sediment profile imaging: An efficient method of remote ecological monitoring of the seafloor (REMOTS™ System). Mar. Ecol. Prog. Ser. 8:115-128.

Rhoads, D.C. and J.D. Germano. 1986. Interpreting long-term changes in benthic community structure: A new protocol. Hydrobiologia. 142:291-308.

Rhoads, D.C. and J.D. Germano. 1990. The use of REMOTS® imaging technology for disposal site selection and monitoring. pp. 50-64. In: Geotechnical Engineering of Ocean Waste Disposal, K. Demars and R. Chaney (eds). ASTM Symposium Volume, January, 1989. Orlando, FL.

Rosenberg, R., H.C. Nilsson, and R.J. Diaz. 2001. Response of benthic fauna and changing sediment redox profiles over a hypoxic gradient. Estuarine, Coastal and Shelf Science 53: 343-350.

Valente, R.M., D.C. Rhoads, J.D. Germano, and V.J. Cabelli. 1992. Mapping of benthic enrichment patterns in Narragansett Bay, RI. Estuaries 15:1-17.

Ziebis, W., Huettel, M., and S. Forster. 1996. Impact of biogenic sediment topography on oxygen fluxes in permeable seabeds. Mar. Ecol. Prog. Ser. 140: 227-237.

FIGURES

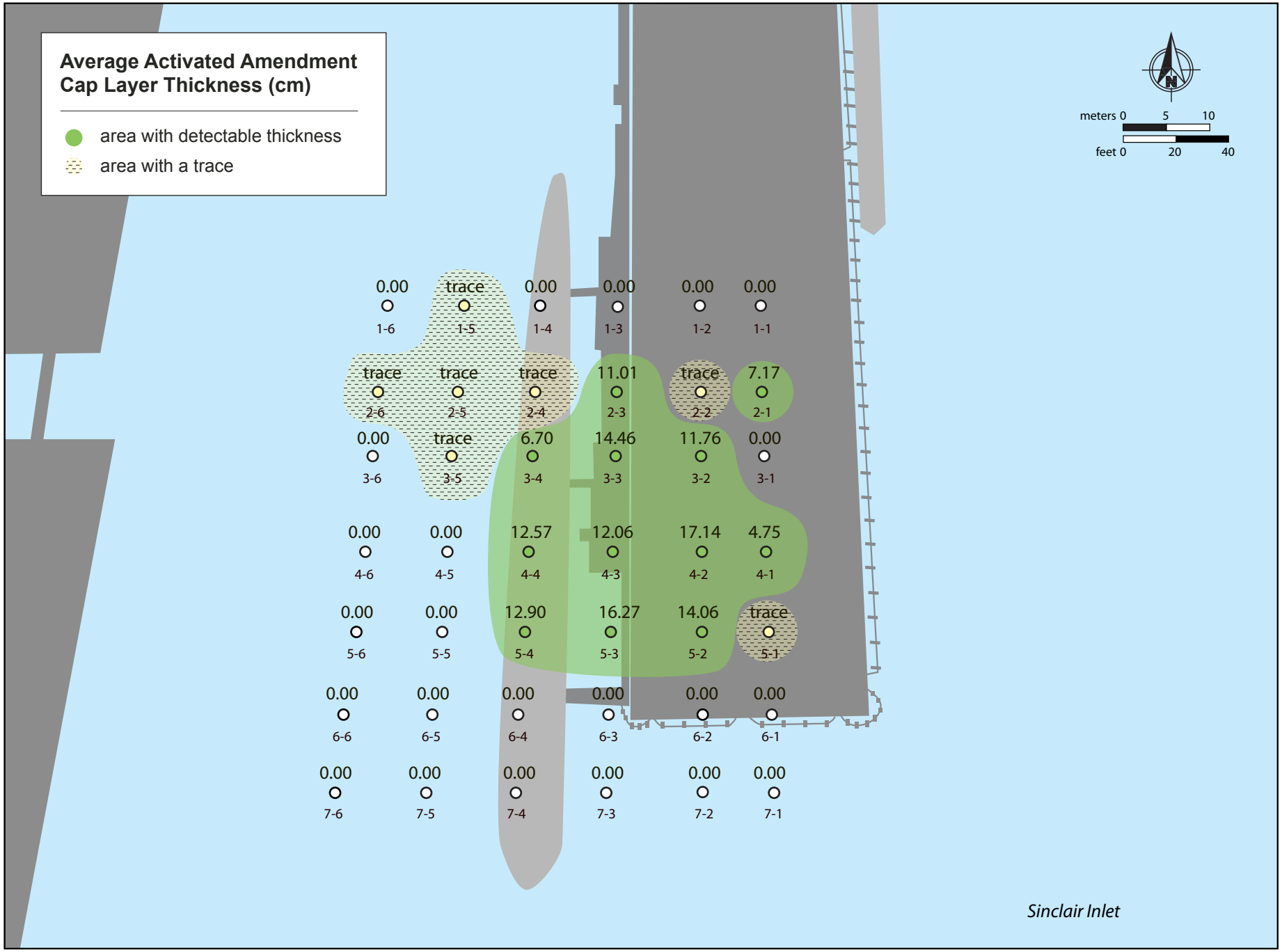

Figure 1: Spatial distribution and average depositional thickness (cm) of the AquaGate +PACTM material placed at locations in and around Pier 7 at the PSNS & IMF Bremerton site in October, 2012.

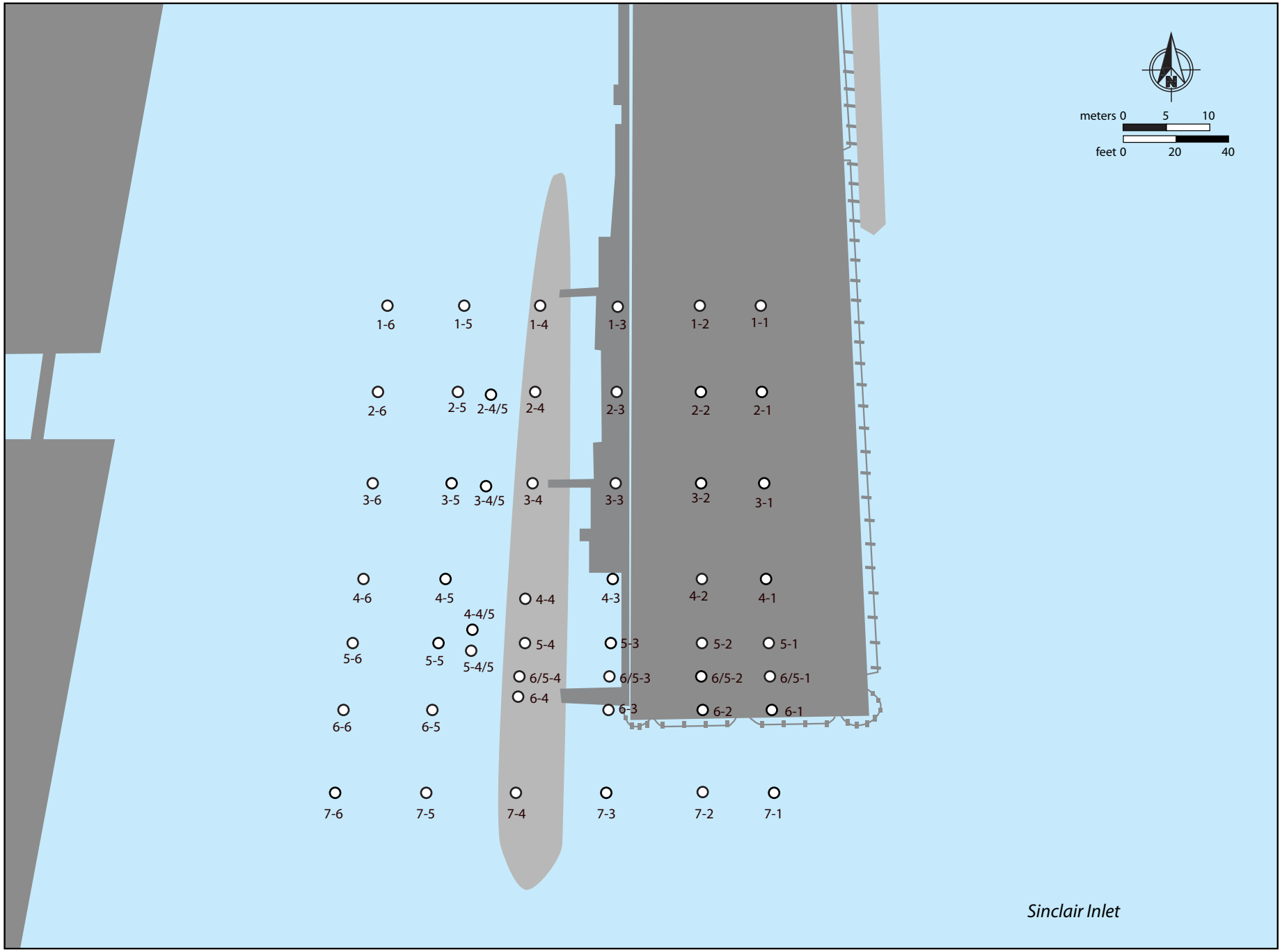

Figure 2: Location of SPI stations sampled under and around Pier 7 at PSNS & IMF, Bremerton site in August 2013.

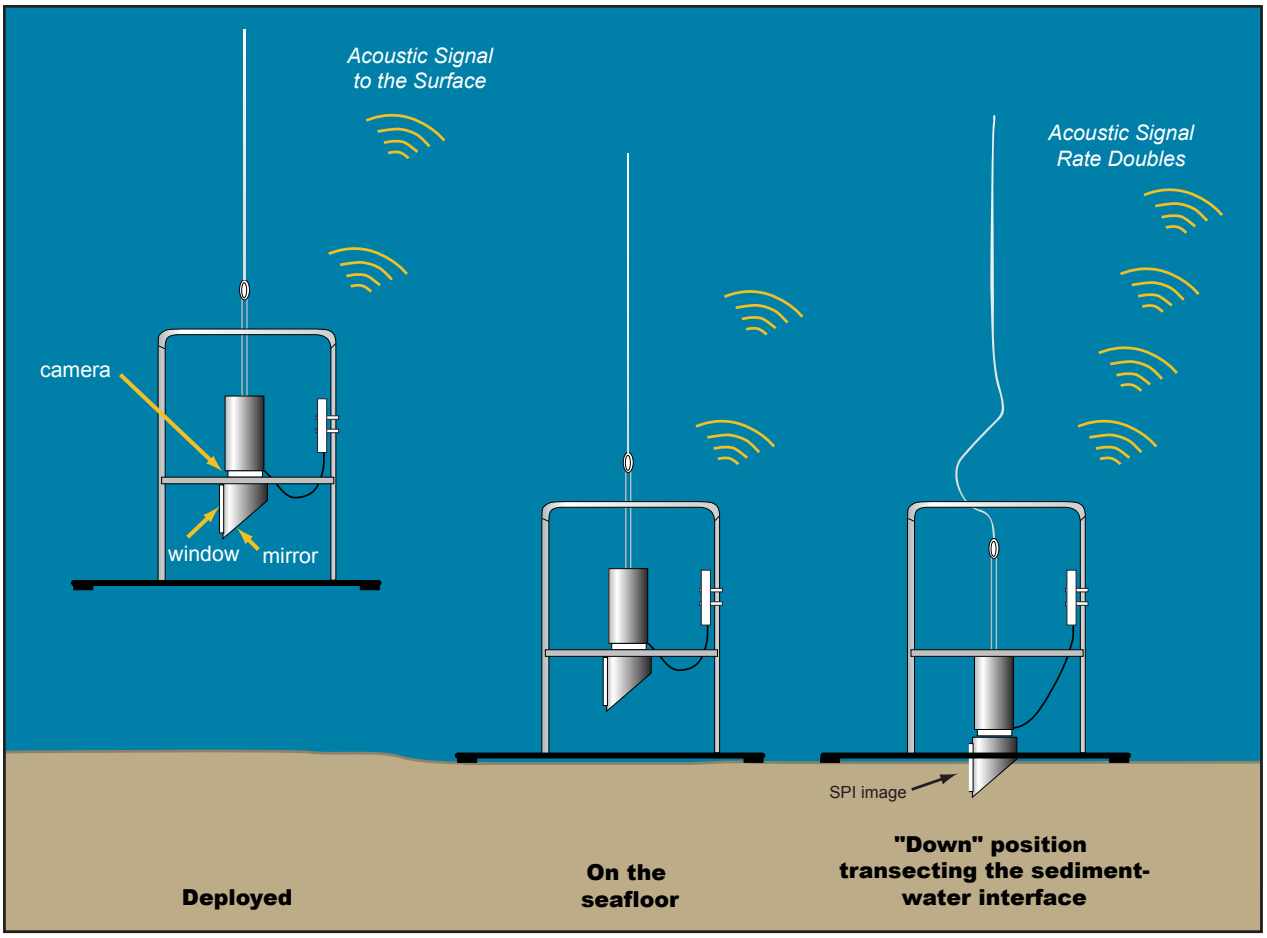

Figure 3: Deployment and operation of the SPI camera system.

Figure 4: The hand-held SPI system used by divers for all stations that were located underneath Pier 7 at PSNS & IMF, Bremerton site.

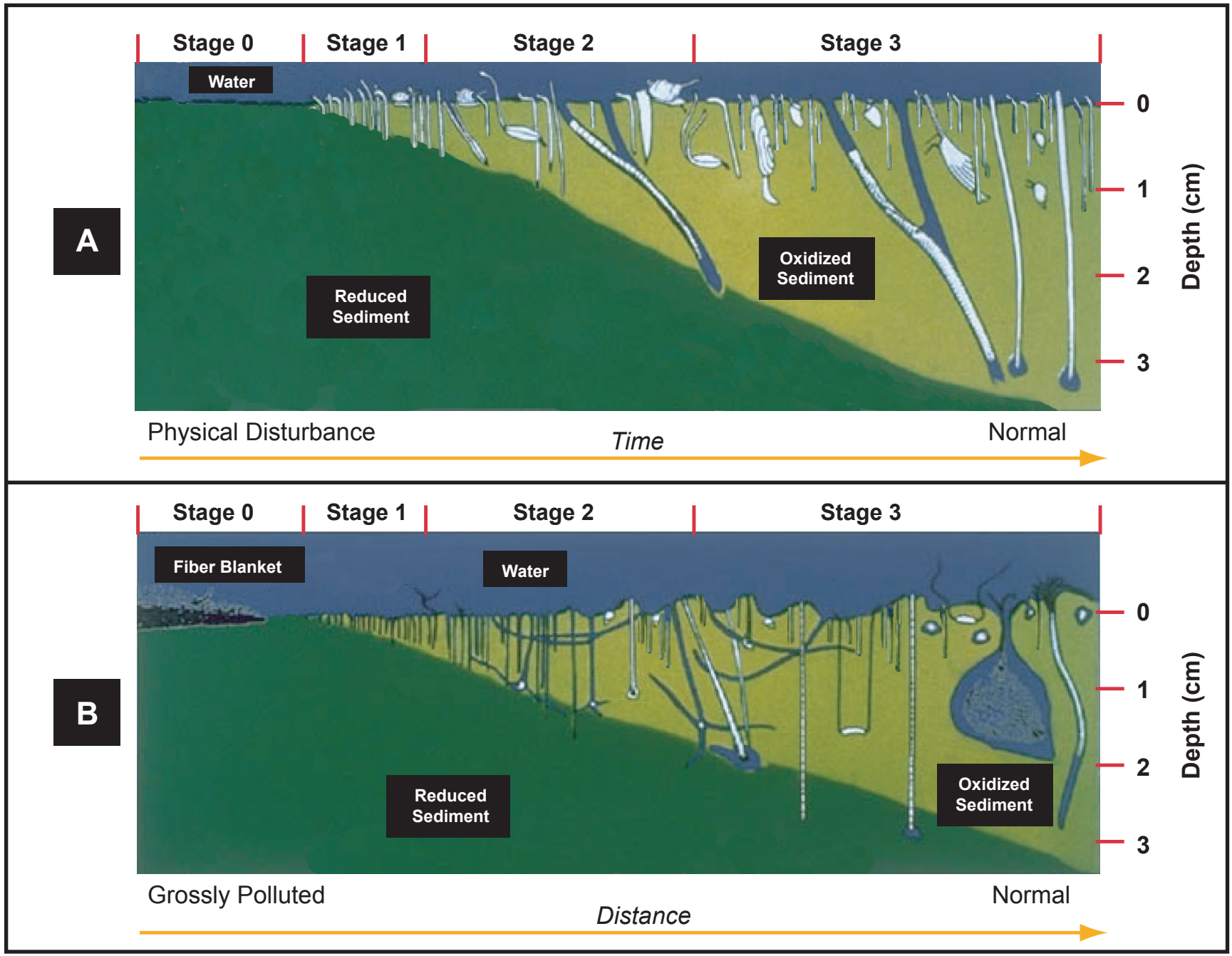

Figure 5: The stages of infaunal succession as a response of soft-bottom benthic communities to physical disturbance (top panel) or organic enrichment (bottom panel). From Rhoads and Germano, 1982.

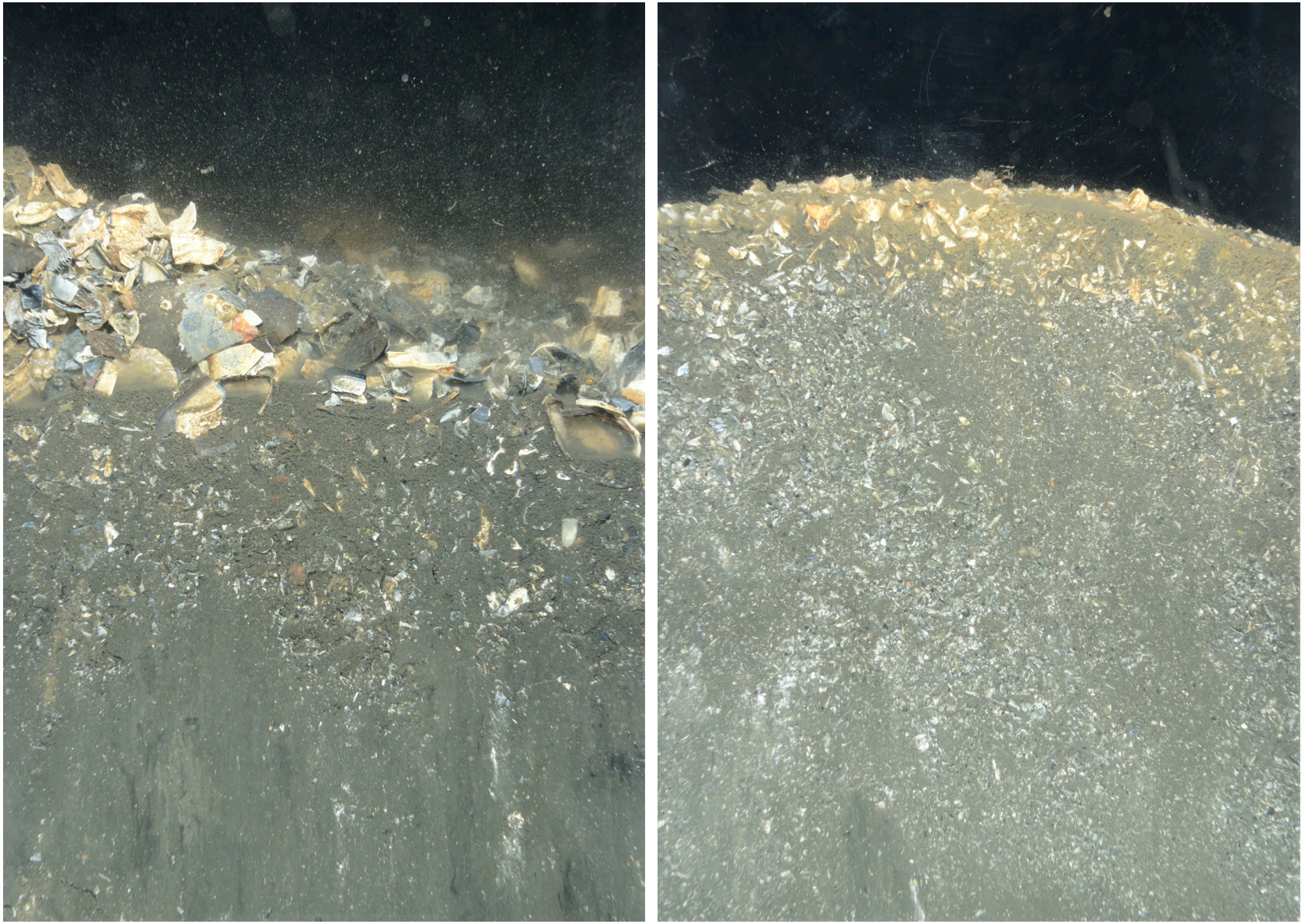

01-1 06-1

Figure 6: These profile images taken with the hand-held camera under the pier from Station 01-1 (left) and Station 06-1 (right) show the unusually high percentage of shell fragments mixed in with the silt-clay sediments; the high shell content was typical for the majority of stations under Pier 7. Scale: width of each profile image = 14.6 cm.

1-3 3-3

Figure 7: These profile images from Stations 1-3 (left) and 3-3 (right) show a shell and cobble armoring layer over the ambient fine sediments. Scale: width of each profile image = 14.6 cm.

1-3

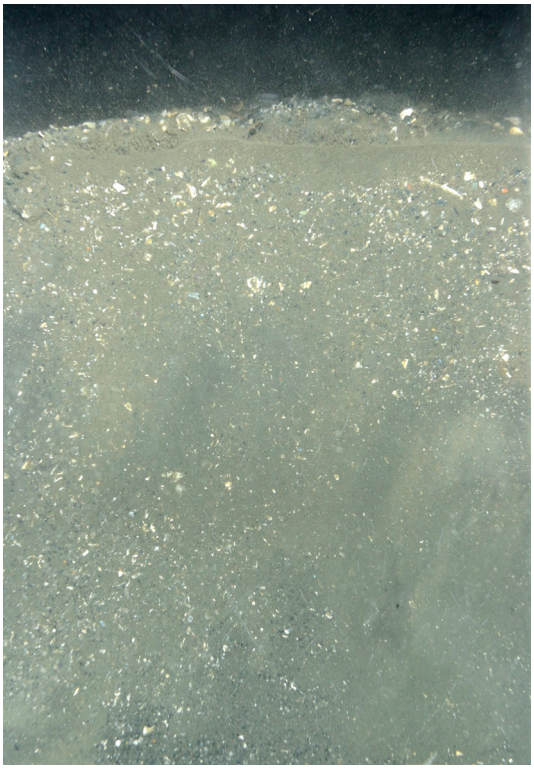

2012

2013

4-3

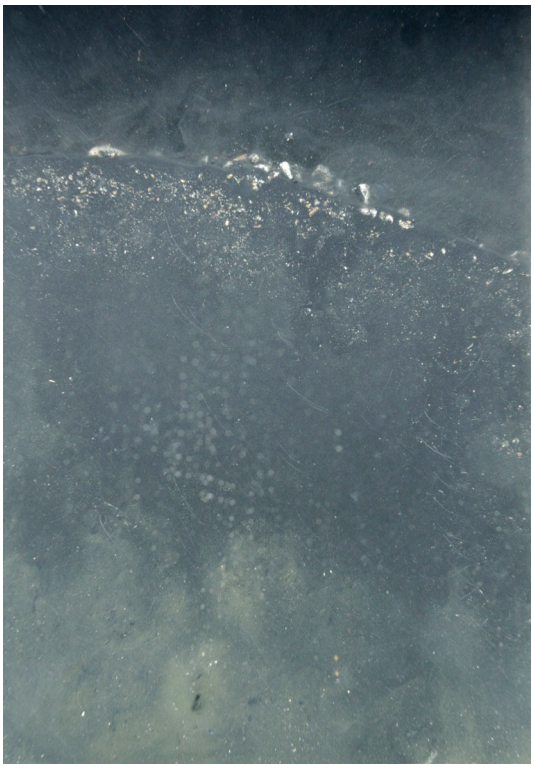

2012

2013

Figure 8: These profile images from the same stations taken in 2012 and 2013 show the radical change in sediment type because of the appearance of the surface armoring of cobble and shell; compare the differences in images from Station 1-3 (top) and 4-3 (bottom). Scale: width of each profile image = 14.6 cm.

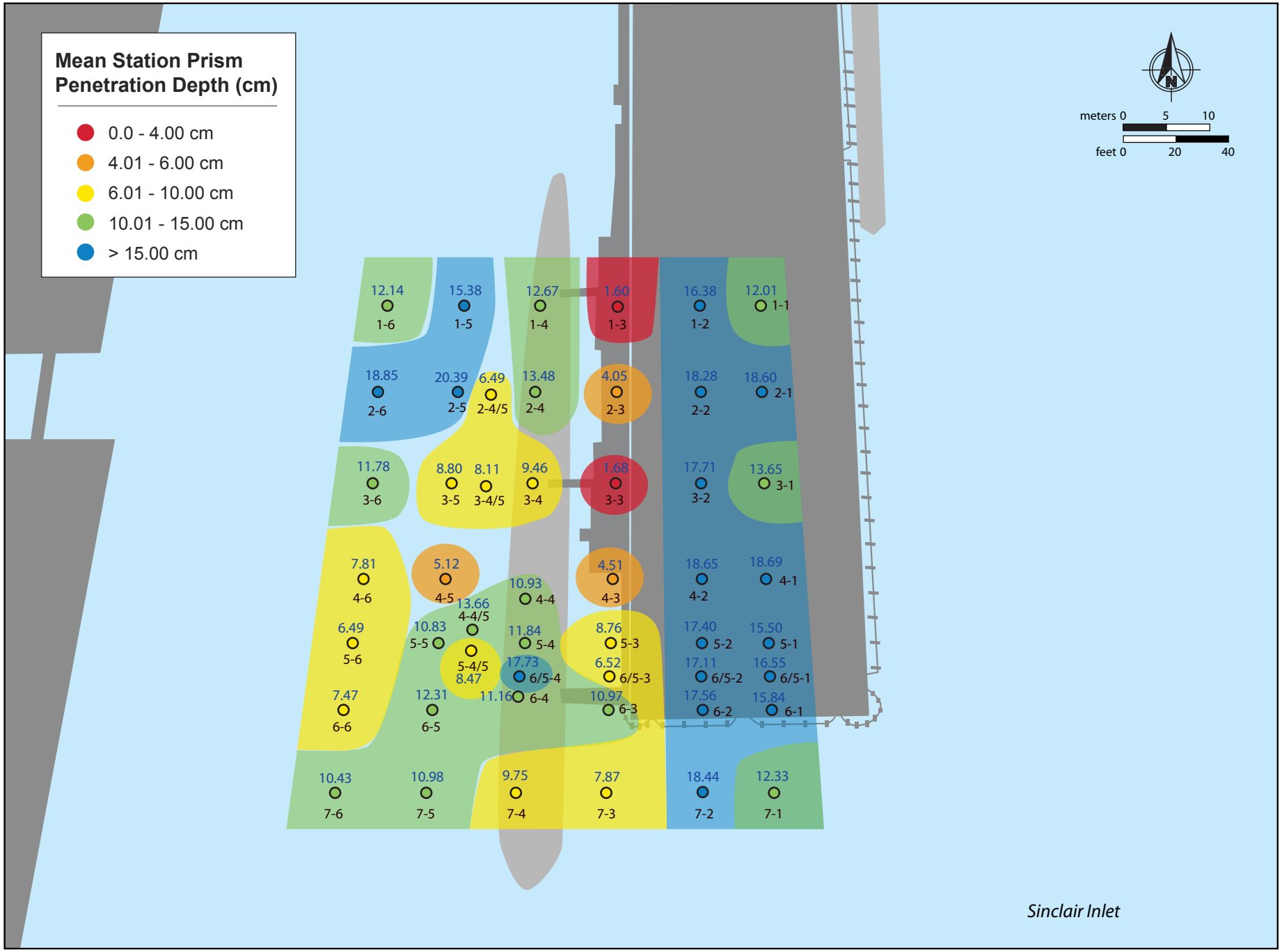

Figure 9: Spatial distribution of mean camera prism penetration depth (cm) at Pier 7 at the PSNS & IMF Bremerton site in August, 2013.

Figure 10: This profile image from Station 5-3 shows a distinct layer of the white pebbles that were coated with the reactive amendment and used as a carrier to get the material to the bottom sediments; particles of activated carbon are still visible in the subsurface profile. Scale: width of profile image = 14.6 cm.

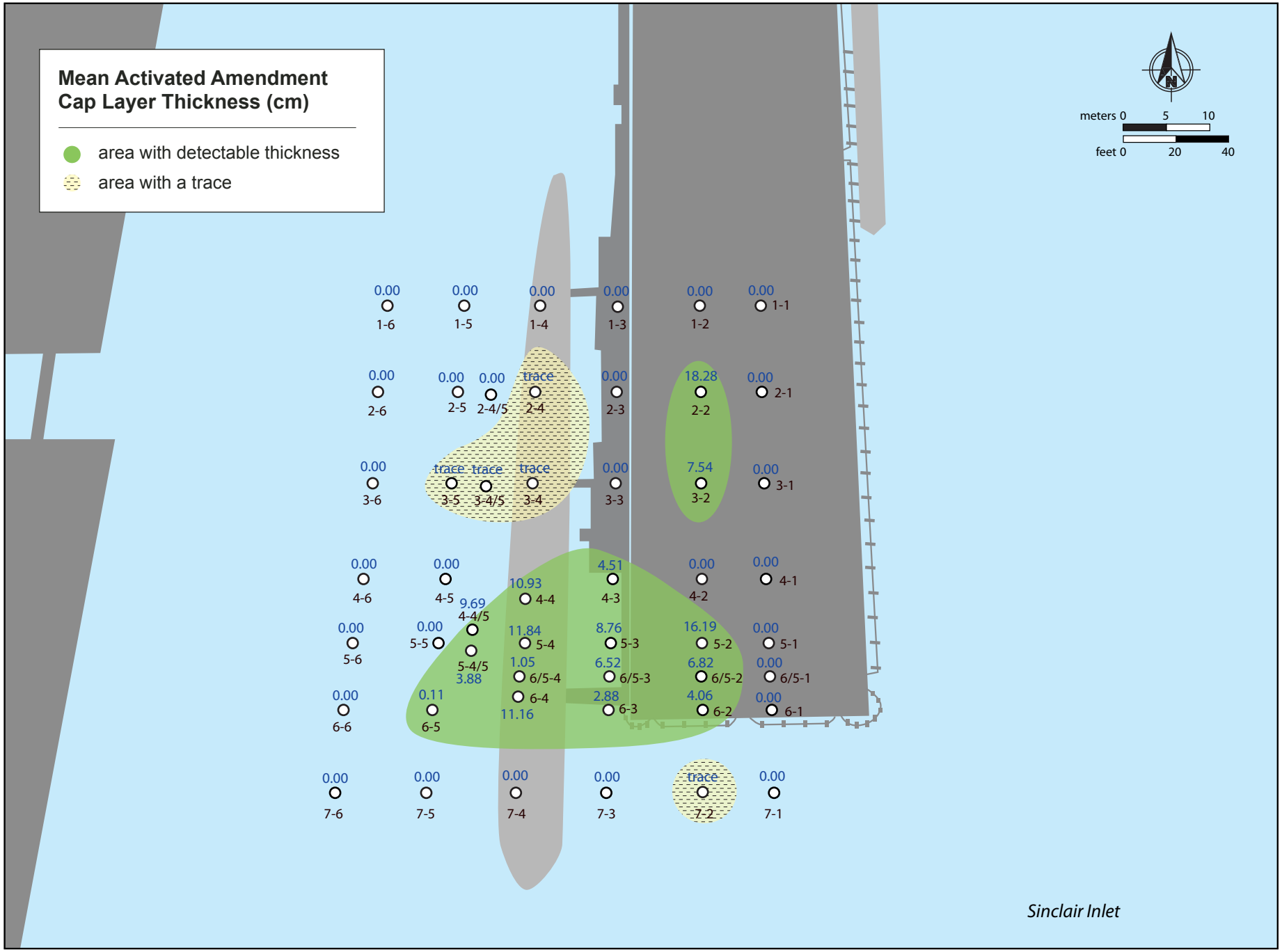

Figure 11: Spatial distribution and mean depositional thickness (cm) of the AquaGate +PACTM material placed at locations in and around Pier 7 at the PSNS & IMF Bremerton site.

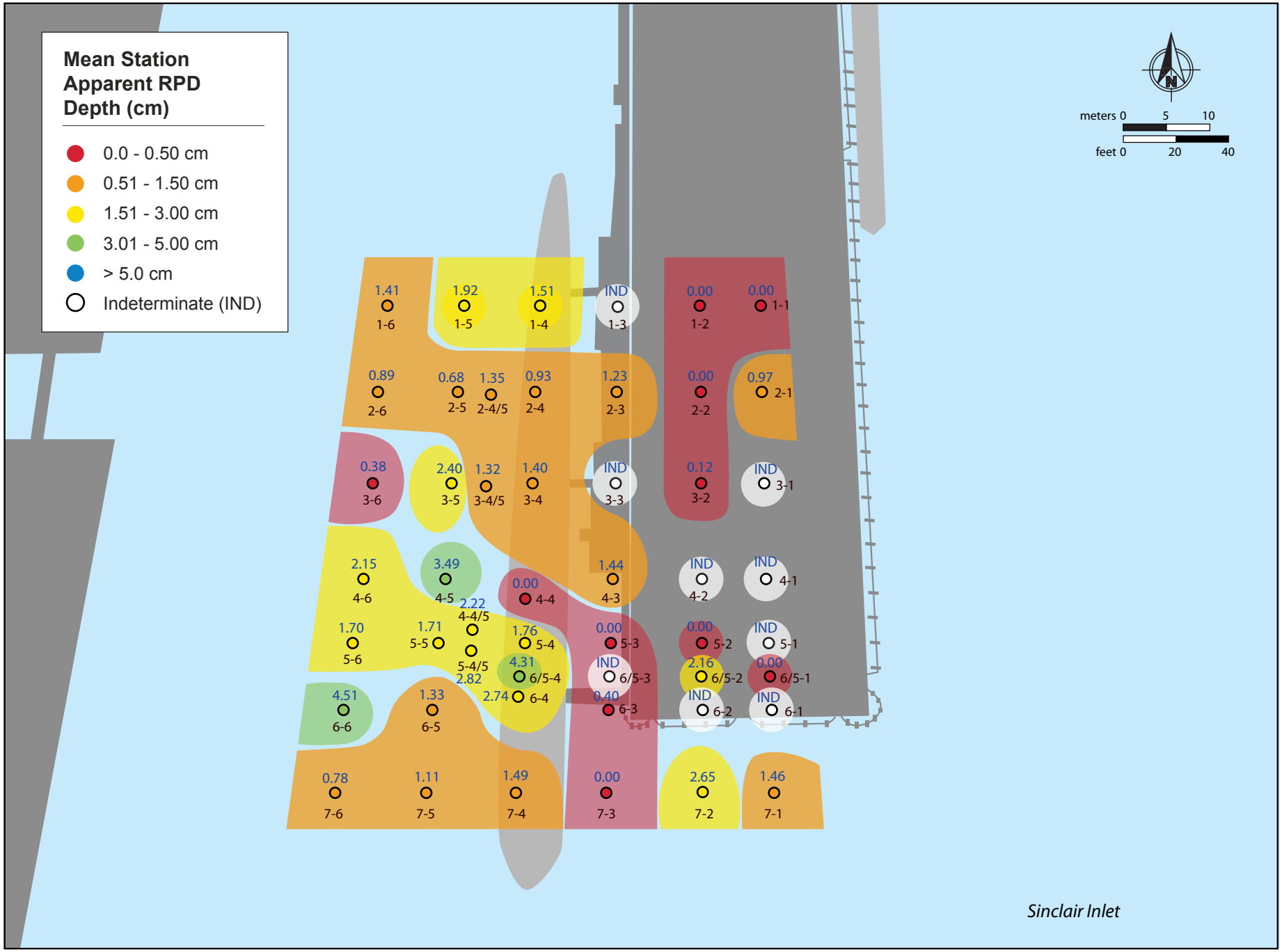

Figure 12: Spatial distribution of mean apparent RPD depth (cm) at Pier 7 in August, 2013.

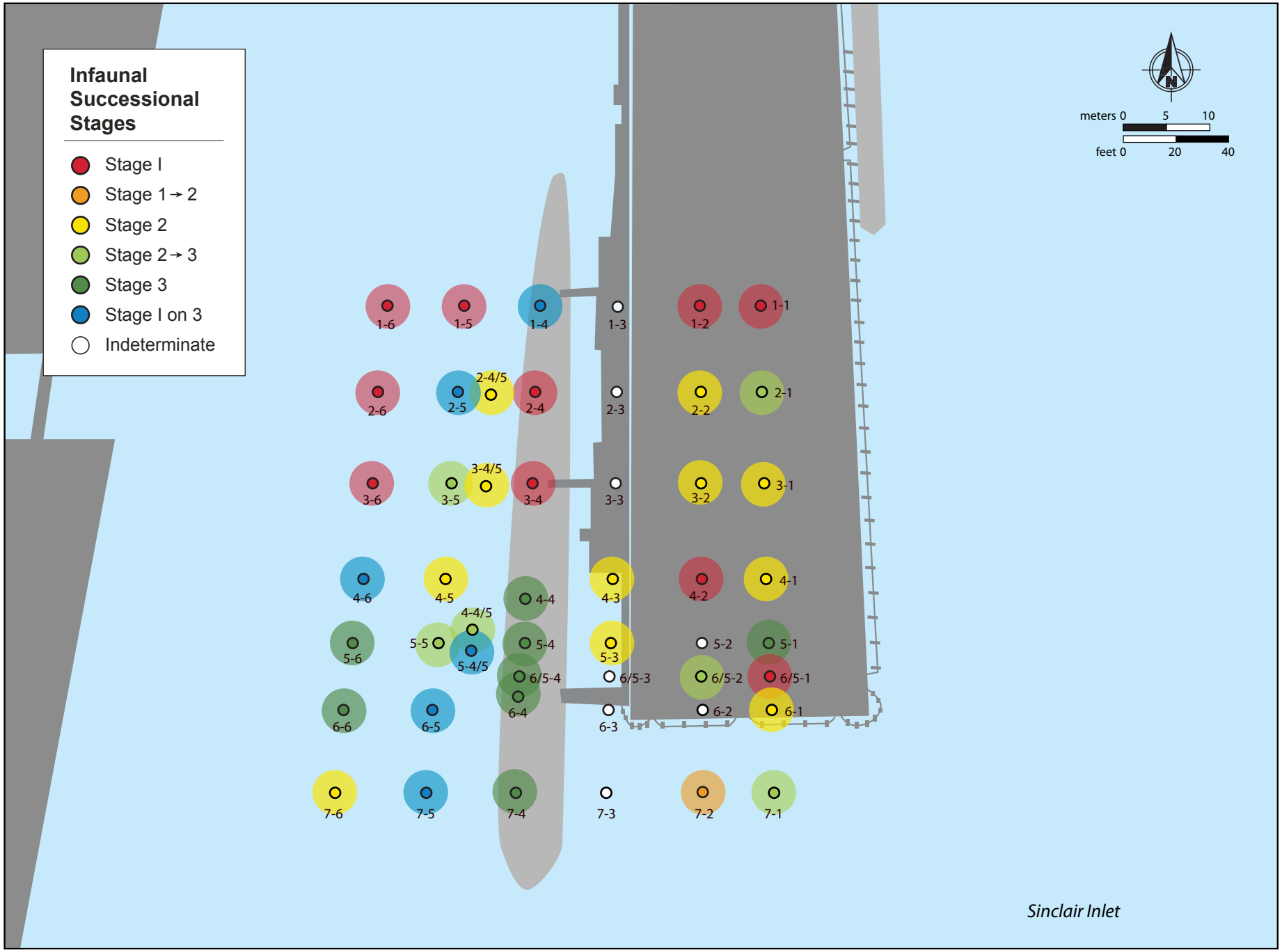

Figure 13: Spatial distribution of infaunal successional stages at Pier 7 in August, 2013.

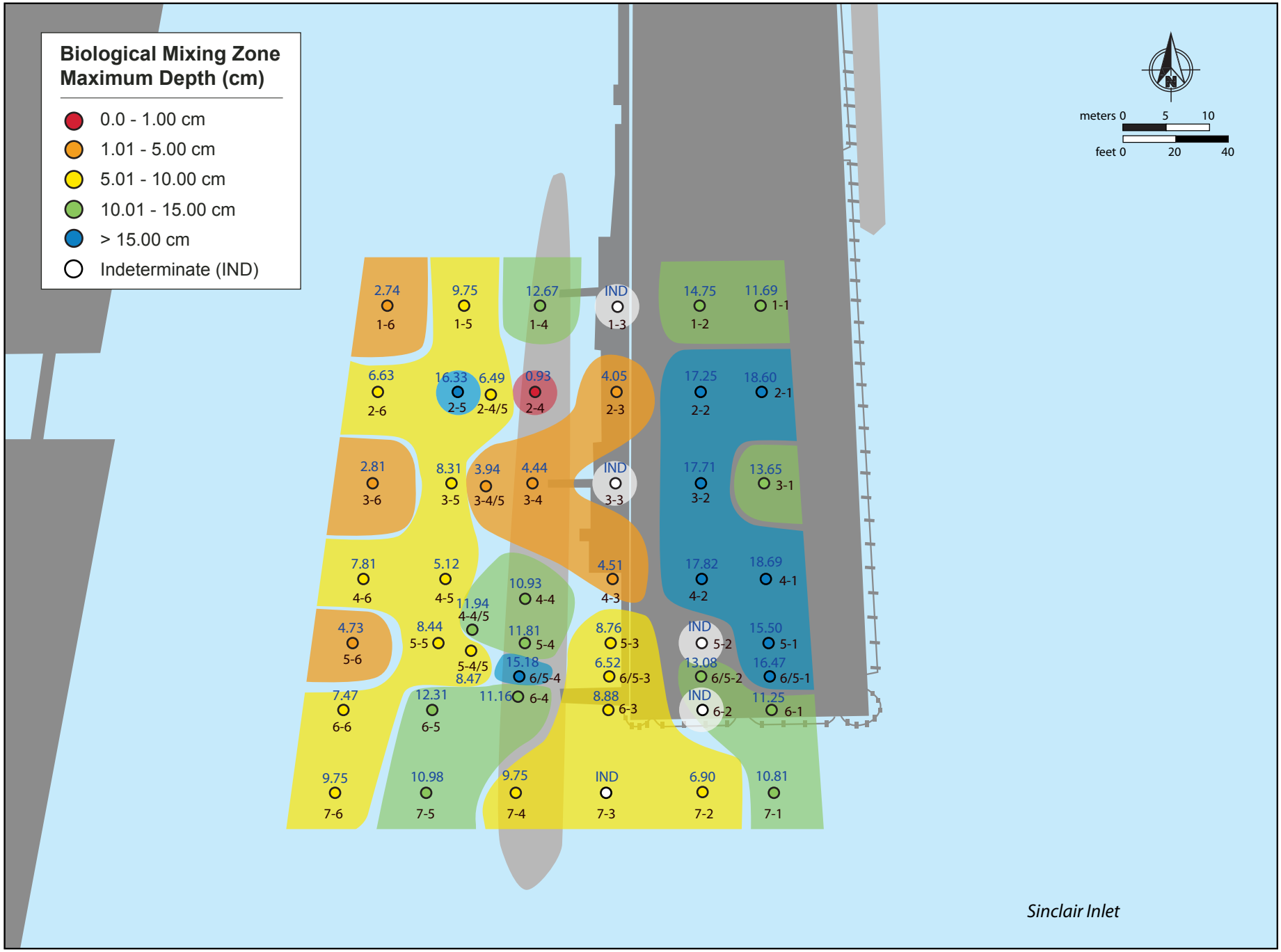

Figure 14: Spatial distribution of maximum biological mixing depth at Pier 7 at the PSNS & IMF Bremerton site in August, 2013.

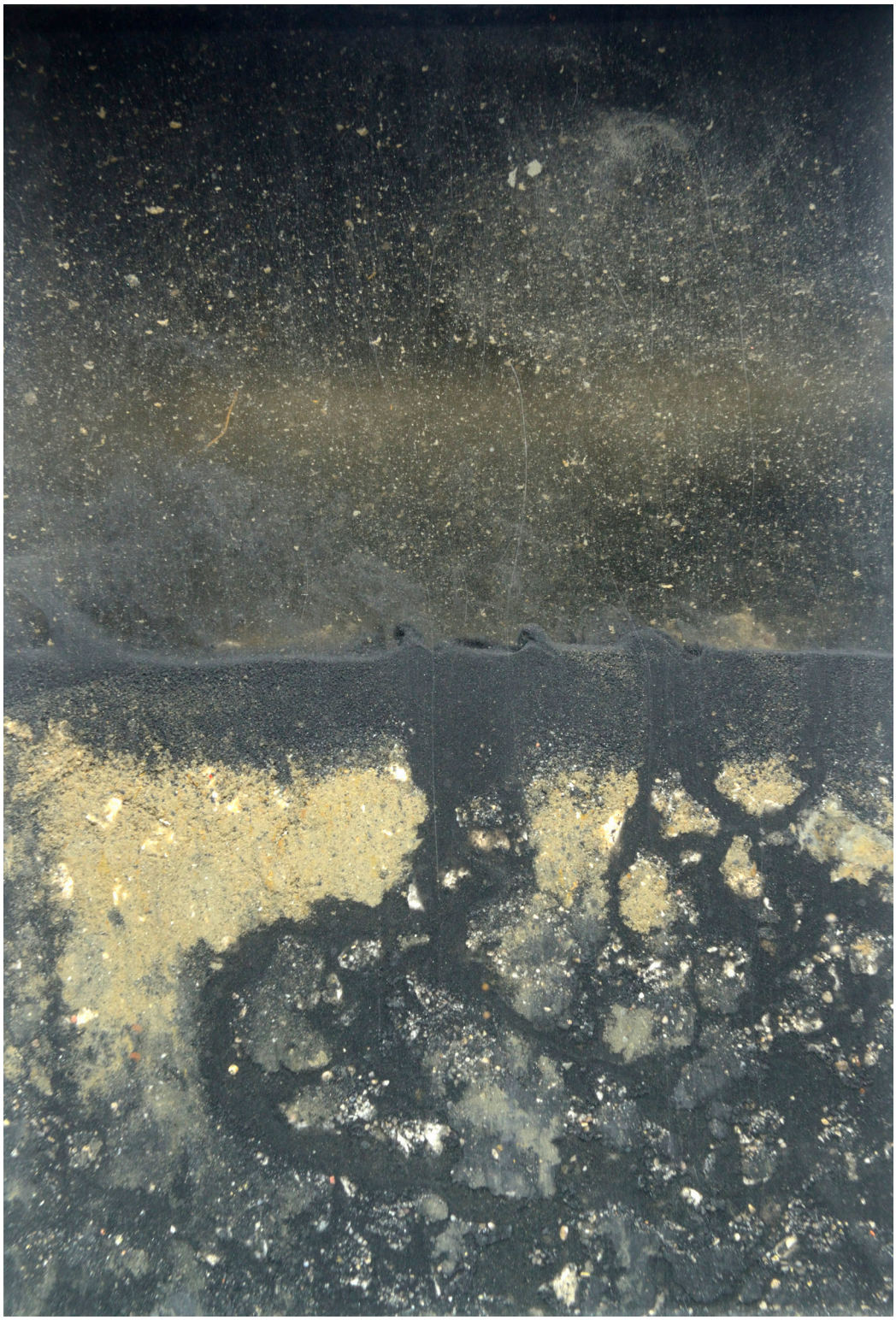

Figure 15: This profile image from Station 4-4 shows active particle transport of the activated carbon particles as well as the development of a surface oxidized layer. Scale: width of profile image = 14.6 cm.

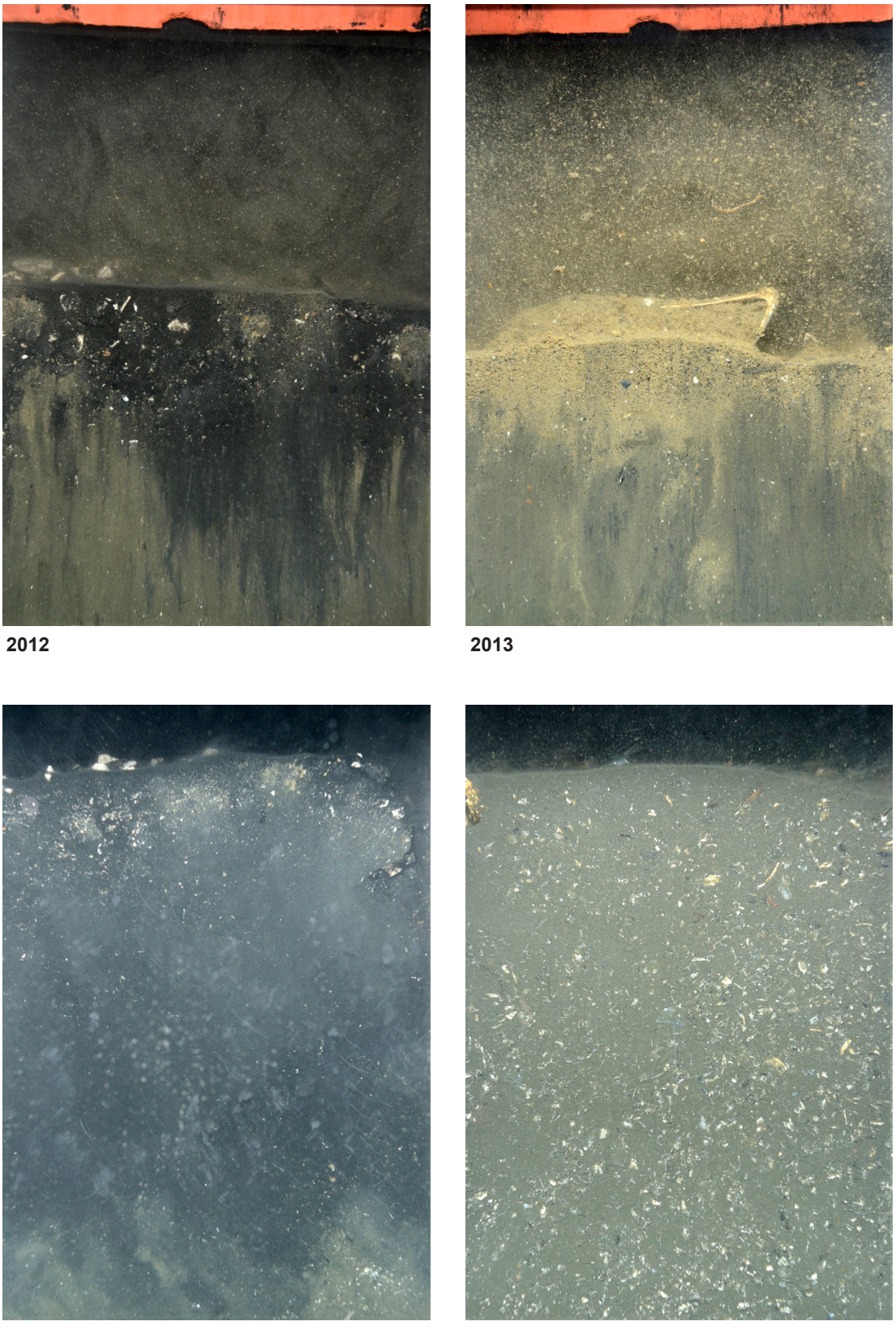

Figure 16: These profile images from Stations 3-4 (top) and 4-2 (bottom) show an obvious presence of the reactive amendment in 2012 that seems to no longer be present in 2013. Scale: width of each image = 14.6 cm.

2012 2013

Figure 17: These profile images from 2012 and 2013 at Station 6-4 show the small-scale heterogeneity in the spatial distribution of the reactive amendment added in Oct 2012. Scale: width of each image = 14.6 cm.

APPENDIX A

Sediment Profile Image Analysis Results

STATION	Frame or HandHeld	Stops	Weights	REP	DATE	TIME	Calibration Constant	Penetration Area (sq.cm)	Average Penetration (cm)	GAC Layer Area (sq.cm)	Mean GAC Layer depth (cm)	RPD Area (sq.cm)	Mean RPD (cm)	Mixing Zone Max Depth (cm)	Successional Stage
1-1	H	-	-	a	8/13/2013	9:04:13	14.624	175.63	12.01	0.00	0.00	0.00	0.00	11.69	Stage 1
1-2	H	-	-	a	8/13/2013	9:06:06	14.624	239.59	16.38	0.00	0.00	0.00	0.00	14.75	Stage 1
1-3	F	15	4	A	8/13/2013	12:25:37	14.580	23.33	1.60	0.00	0.00	ind	ind	ind	indeterminate
1-4	F	17	4	D	8/14/2013	9:16:45	14.580	184.72	12.67	0.00	0.00	22.04	1.51	12.67	Stage 1 on 3
1-5	F	15	2	B	8/14/2013	9:21:54	14.580	224.17	15.38	0.00	0.00	28.04	1.92	9.75	Stage 1
1-6	F	15	2	B	8/14/2013	9:26:40	14.580	176.98	12.14	0.00	0.00	20.59	1.41	2.74	Stage 1
2-1	H	-	-	E	8/13/2013	9:33:08	14.624	272.01	18.60	0.00	0.00	14.24	0.97	18.60	Stage 2 ->3
2-2	H	-	-	A	8/13/2013	9:35:00	14.624	267.30	18.28	267.30	18.28	0.00	0.00	17.25	Stage 2
2-3	F	15	4	B	8/13/2013	12:20:39	14.580	59.00	4.05	0.00	0.00	17.93	1.23	4.05	indeterminate
2-4	F	15	2	B	8/14/2013	9:43:06	14.580	196.52	13.48	trace	trace	ind	0.93	0.93	Stage 1
2-4/5	F	15	2	A	8/14/2013	9:44:55	14.580	94.60	6.49	0.00	0.00	19.73	1.35	6.49	Stage 2
2-5	F	15	2	B	8/14/2013	9:49:49	14.580	297.27	20.39	0.00	0.00	9.92	0.68	16.33	Stage 1 on 3
2-6	F	15	2	A	8/14/2013	9:54:41	14.580	274.85	18.85	0.00	0.00	12.92	0.89	6.63	Stage 1
3-1	H	-	-	A	8/13/2013	9:57:33	14.624	199.55	13.65	0.00	0.00	ind	ind	13.65	Stage 2
3-2	H	-	-	A	8/13/2013	9:59:30	14.624	258.92	17.71	110.23	7.54	1.72	0.12	17.71	Stage 2
3-3	F	15	4	C	8/13/2013	12:15:56	14.580	24.50	1.68	0.00	0.00	ind	ind	ind	indeterminate
3-4	F	15	2	B	8/14/2013	10:17:55	14.580	137.91	9.46	trace	trace	20.36	1.40	4.44	Stage 1
3-4/5	F	15	2	B	8/14/2013	10:21:03	14.580	118.28	8.11	trace	trace	19.19	1.32	3.94	Stage 2
3-5	F	15	2	B	8/14/2013	10:24:35	14.580	128.35	8.80	trace	trace	34.95	2.40	8.31	Stage 2 ->3
3-6	F	15	2	B	8/14/2013	10:28:22	14.580	171.75	11.78	0.00	0.00	5.58	0.38	2.81	Stage 1
4-1	H	-	-	A	8/13/2013	10:03:12	14.624	273.35	18.69	0.00	0.00	ind	ind	18.69	Stage 2
4-2	H	-	-	A	8/13/2013	10:04:55	14.624	272.77	18.65	0.00	0.00	ind	ind	17.82	Stage 1
4-3	F	15	4	B	8/13/2013	12:03:31	14.580	65.78	4.51	-	4.51	ind	1.44	4.51	Stage 2
4-4	F	15	2	A	8/14/2013	10:40:01	14.580	159.38	10.93	-	10.93	0.00	0.00	10.93	Stage 3
4-4/5	F	15	2	A	8/14/2013	10:48:54	14.580	199.22	13.66	141.33	9.69	ind	2.22	11.94	Stage 2 ->3
4-5	F	15	2	B	8/14/2013	10:56:45	14.580	74.65	5.12	0.00	0.00	ind	3.49	5.12	Stage 2
4-6	F	15	2	B	8/14/2013	11:01:49	14.580	113.90	7.81	0.00	0.00	31.41	2.15	7.81	Stage 1 on 3
5-1	H	-	-	B	8/13/2013	10:08:19	14.624	226.71	15.50	0.00	0.00	ind	ind	15.50	Stage 3
5-2	H	-	-	B	8/13/2013	10:10:56	14.624	254.47	17.40	236.73	16.19	0.00	0.00	ind	indeterminate
5-3	F	15	4	B	8/13/2013	11:57:24	14.580	127.78	8.76	-	8.76	0.00	0.00	8.76	Stage 2
5-4	F	15	2	B	8/14/2013	10:45:39	14.580	172.70	11.84	-	11.84	ind	1.76	11.81	Stage 3
5-4/5	F	15	2	A	8/14/2013	10:52:38	14.580	123.47	8.47	56.57	3.88	41.11	2.82	8.47	Stage 1 on 3
5-5	F	15	2	B	8/14/2013	11:11:50	14.580	157.90	10.83	0.00	0.00	24.98	1.71	8.44	Stage 2 ->3
5-6	F	15	2	B	8/14/2013	11:06:22	14.580	94.68	6.49	0.00	0.00	24.79	1.70	4.73	Stage 3

STATION	Frame or HandHeld	Stops	Weights	REP	DATE	TIME	Calibration Constant	Penetration Area (sq.cm)	Average Penetration (cm)	GAC Layer Area (sq.cm)	Mean GAC Layer depth (cm)	RPD Area (sq.cm)	Mean RPD (cm)	Mixing Zone Max Depth (cm)	Successional Stage
6-1	H	-	-	B	8/13/2013	10:45:09	14.624	231.68	15.84	0.00	0.00	ind	ind	11.25	Stage 2
6-2	H	-	-	A	8/13/2013	10:46:33	14.624	256.82	17.56	59.41	4.06	ind	ind	ind	indeterminate
6-3	H	-	-	B	8/13/2013	11:11:03	14.624	160.44	10.97	42.16	2.88	5.89	0.40	8.88	indeterminate
6-4	F	15	3	A	8/14/2013	11:37:37	14.580	162.74	11.16	-	11.16	ind	2.74	11.16	Stage 3
6-5	F	15	3	B	8/14/2013	12:01:07	14.580	179.55	12.31	1.64	0.11	19.35	1.33	12.31	Stage 1 on 3
6-6	F	15	3	C	8/14/2013	12:12:54	14.580	108.89	7.47	0.00	0.00	65.73	4.51	7.47	Stage 3
6/5-1	H	-	-	A	8/13/2013	10:13:00	14.624	242.05	16.55	0.00	0.00	0.00	0.00	16.47	Stage 1
6/5-2	H	-	-	B	8/13/2013	10:14:58	14.624	250.19	17.11	99.74	6.82	ind	2.16	13.08	Stage 2 ->3
6/5-3	F	15	4	B	8/13/2013	11:51:00	14.580	95.04	6.52	95.04	6.52	ind	ind	6.52	indeterminate
6/5-4	F	15	3	B	8/14/2013	11:49:20	14.580	258.55	17.73	15.38	1.05	62.82	4.31	15.18	Stage 3
7-1	H	-	-	B	8/13/2013	10:52:04	14.624	180.31	12.33	0.00	0.00	21.42	1.46	10.81	Stage 2 ->3
7-2	H	-	-	B	8/13/2013	10:55:17	14.624	269.68	18.44	trace	trace	38.76	2.65	6.90	Stage 1 -> 2
7-3	H	-	-	B	8/13/2013	11:08:36	14.624	115.06	7.87	0.00	0.00	0.00	0.00	ind	indeterminate
7-4	F	15	3	A	8/14/2013	11:55:00	14.580	142.15	9.75	0.00	0.00	21.70	1.49	9.75	Stage 3
7-5	F	15	3	A	8/14/2013	12:03:03	14.580	160.02	10.98	0.00	0.00	16.15	1.11	10.98	Stage 1 on 3
7-6	F	15	3	A	8/14/2013	12:07:50	14.580	152.04	10.43	0.00	0.00	11.42	0.78	9.75	Stage 2

STATION	Frame or HandHeld	Stops	Weights	REP	COMMENT
1-1	H	-	-	a	polychaetes
1-2	H	-	-	a	Silty sed; no GAC; shells (mussels) and shell fragments on surface at below SWI throughout depth; no clear aRPD; small polychaetes visible at depth
1-3	F	15	4	A	Silty sand, no GAC; surface covered with large pebbles/rocks and shell fragments, penetration too shallow to determine bio mixing or stage
1-4	F	17	4	D	Silty sed; no GAC; debris in background, fecal pellet layer at SWI; patchy aRPD, evidence of burrowing at depth.
1-5	F	15	2	B	Silty sed; no GAC; small to medium mud clasts (camera base sled artifact) on surface; finer grains at SWI; patchy, thin aRPD
1-6	F	15	2	B	Silty sed; no GAC; homogeneous texture with little reworking at depth
2-1	H	-	-	E	Silty sand; no GAC; several large shell halves at surface, smaller shell frag throughout depth; bit of algal below depth; layer of fine sed particles on surface; discontinuous patchy aRPD; evidence of burrowing, infauna visible on right and burrowing to depth of profile (worm at lower left corner)
2-2	H	-	-	A	GAC incorporated throughout depth, thicker/darker near SWI; shell fragments and white pebbles on surface; shell frag and debris incorporated in upper ~6-8cm; clear small burrows at depth and to right of center
2-3	F	15	4	B	Silty sed; no GAC; penetration depth too shallow to determine successional stage; mussel shells, shell fragments, fecal pellets and debris on surface.
2-4	F	15	2	B	Silty sed; trace GAC on white pebbles in dragged down/collapsed section on right; few bits of debris and crab carapace on surface; large bivalve shell dragged down in collapsed section on right; thin aRPD; some fecal pellets at SWI
2-4/5	F	15	2	A	Silty very fine sand; no GAC; some fecal pellets on surface; evidence of burrowing at depth
2-5	F	15	2	B	Silty sed; no GAC; thin layer of fine reduced sed at SWI; patchy aRPD; void at ~5 cm, evidence of burrow opening at 16 cm
2-6	F	15	2	A	Silty sed; no GAC; bits of organic debris on surface; very homogeneous texture
3-1	H	-	-	A	Silty sand, no GAC; few shell fragments on surface, cable/cord on surface (from divers); finer grains at surface; aRPD hidden by profile disturbance during prism insertion; v. small shell frag and debris throughout depth; small burrows throughout depth of profile
3-2	H	-	-	A	Silty sed; GAC mixed with sediment grains in upper 2 cm, GAC visible through much of profile (partly due to sampling artifact) ; shell fragments and white pebbles on surface; aRPD is patchy, burrowing evident through depth of profile
3-3	F	15	4	C	Cobble bottom over silty sand, no GAC; surface covered with barnacle-encrusted cobble and a few shells, v. shallow penetration
3-4	F	15	2	B	Silty sed; no GAC; signs of burrowing in aRPD; large shell on surface
3-4/5	F	15	2	B	Silty sed, coarser grains near SWI; possible GAC traces at depth; some fecal pellets at surface.
3-5	F	15	2	B	Silty sed; bit of trace GAC on right at depth; coarser grains and fecal pellets at SWI; polychaete at 4.5 cm on right
3-6	F	15	2	B	Silty sand; no GAC; small burrow on left at 2.81cm
4-1	H	-	-	A	Silty sand, no GAC; shell frag and debris on surface and incorporated throughout depth; no clear aRPD; large Sabellid tube gainst faceplate at SWI; small burrow at 10 cm between center and right edge of image as well as small burrows evident at base of profile
4-2	H	-	-	A	Silty sand; no GAC; somewhat finer grains at SWI; shell against faceplate at far left; few bits of debris at surface; shell fragments incorporated densely through depth; small burrows evident throughout profile
4-3	F	15	4	B	Silty sed; coarser grains near surface at right; GAC incorporated with sediment through depth; white pebbles and a few large shells on surface, evidence of burrowing throughout profile; Stage 3 taxa likely present but in very low density
4-4	F	15	2	A	Very fine sandy silt with layer of very fine GAC in upper 1-2cm, followed by ~1-2 cm of oxidized sed with GAC pebbles visible, with 'channels' of GAC through; GAC incorporated with sed through depth from bioturbation; classic photo.
4-4/5	F	15	2	A	Very fine sandy silt with GAC fine carbon particles at surface; GAC throughout depth, thin layer ~1-2cm at SWI, followed by patches of oxidized sediment; then GAC incorporated with sediment as seen by darker stratum mid-profile depth
4-5	F	15	2	B	Silty fine sand; no substantial GAC; shallow penetration; aRPD extends below pen depth; few coarser GAC carrier pebbles on surface in background
4-6	F	15	2	B	Silty sed; no GAC; pit from SWI to ~3cm on right; few pebbles and one large rock on surface; white pebbles on surface in background
5-1	H	-	-	B	Silty sand; no GAC; fine grains at surface; large shell fragments and debris at surface, including what may be former sabellid tube; shell frag incorporated throughout depth; tube of a kind (possibily maldanid tube) extending into sed ~6cm, just to left of center; thin burrows at ~5 and ~10 cm
5-2	H	-	-	B	Silt sed; GAC layer thicker/darker in upper few cm, present almost to base of profile and incorporated at depth (possibly due to sampling artifact); some white pebbles and bits of shell frag at surface and throughout depth; profile too disturbed by samplling to determine successional stage or mixing depth; clear tubing on surface (from divers)
5-3	F	15	4	B	Silty sed; GAC throughout depth, mixed with some coarser grains throughout; surface covered with white GAC carrier pebbles, burrowing throughout depth of profile
5-4	F	15	2	B	Silty sed; GAC throughout depth; few white GAC carrier pebbles and shell fragments on surface; thin layer of GAC at surface; aRPD estimated by linear measurement; GAC incorporated with sed throughout rest of depth; void on left just below SWI
5-4/5	F	15	2	A	Silty sed; few white GAC carrier pebbles on surface; GAC throughout depth, fine layer of activated carbon at SWI from biogenic mounding, incorporated throughout depth below aRPD layer; signs of burrowing throughout profile
5-5	F	15	2	B	Silty sand; no GAC; large shell on surface; fecal pellets at SWI; low density of subsurface burrowing
5-6	F	15	2	B	Silty sand; no GAC; uneven surface; coarser grains near surface; organic debris on surface and in suspension; two small voids to right of center

STATION	Frame or HandHeld	Stops	Weights	REP	COMMENT
6-1	H	-	-	B	Silty sand; no GAC; high density of shell fragments on surface; thin 0.5cm layer of fecal pellets, at SWI, followed by 6+cm of dense shell fragments; worm visible at depth against faceplate
6-2	H	-	-	A	Silty sed; GAC on surface with the finer carbon particles smeared down through profile by sampling artifact; many parameters impossible to measure because of disturbance by divers inserting prism. Many small shell frag incorporated in upper 9 cm
6-3	H	-	-	B	Silty sed; GAC pebbles aggregated on surface with shell fragments; profile too disturbed to determine successional stage accurately
6-4	F	15	3	A	Silty sed; GAC throughout depth; very fine GAC particles in upper cms; few small white GAC carrier pebbles in upper cms; burrowing throughout profile, aRPD linear measurement
6-5	F	15	3	B	Silty sed, coarser grains near SWI; small patch of GAC near SWI on left; few tubes at surface; polychaetes at depth
6-6	F	15	3	C	Silty fine to medium sand, sand ripple near center; clear segmented polychaete tube above SWI on left; aRPD extends beyond depth on left; 3 small polychaetes against faceplate ~ 5-6 cm
6/5-1	H	-	-	A	Silty sand; no GAC, no aRPD; small burrows at depth, possible Stage 2 fauna is present but not distinct
6/5-2	H	-	-	B	Silty sed; GAC pebbles on surface with shell fragments, worm visible at depth on right; aRPD determined by linear measurement, top layer disturbed by prism movement
6/5-3	F	15	4	B	Silty sed; GAC throughout depth, patches of aRPD below ~4cm layer of white pebbles, impossible to determine accurately due to profile disturbance from fine particles falling inbetween coarse GAC carrier pebbles & faceplate
6/5-4	F	15	3	B	Silty sed; GAC carrier pebble at depth (dragdown by prism); uneven surface; aRPD continues in dragdown, chaotic mix; algal debris on surface at left and in dragdown; small void or burrow opening at right ~9cm, evidence of burrow at left at 15cm
7-1	H	-	-	B	Silty sed; no GAC; shells and crab carapaces on surface; finer grain layer at surface; two retracted anemones at depth, subsurface burrows evident
7-2	H	-	-	B	Silty sand, coarser grains at surface; some shell fragments and GAC pebbles on surface; small polychaete (capatellid) just below aRPD on right
7-3	H	-	-	B	Silty sed, no GAC; surface completely covered with shell fragments with smaller shell fragments incorporated through depth
7-4	F	15	3	A	Silty sed; no GAC; uneven surface; fecal pellets at SWI; burrowing anemone at depth to 8.66cm
7-5	F	15	3	A	Silty sed, some coarser grains near SWI; no GAC; sabellid tube at far left and through sed; ~5 shrimp on surface
7-6	F	15	3	A	Silty sed; no GAC; few bits of small shell fragments and organic debris on surface; small polychaetes visible against faceplate just below aRPD in center